Construction and Building Materials 75 (2015) 144–156

Contents lists available at ScienceDirect

Construction and Building Materials

journal homepage: www.elsevier.com/locate/conbuildmat

Influence of shrinkage on compressive behavior of concrete-filled FRP tubes: An experimental study on interface gap effect

Thomas Vincent, Togay Ozbakkaloglu *

School of Civil, Environmental and Mining Engineering, University of Adelaide, Australia

HIGHLIGHTS

- 30 FRP-confined normal- and high-strength concrete specimens are experimentally tested.
- Shrinkage strains in normal- and high-strength concrete-filled FRP tubes are reported.
- Effects of five different concrete shrinkage levels on compressive behavior are investigated.
- Axial stress–strain and corresponding lateral-to-axial strain curves are presented.
- Ultimate conditions are tabulated and key confinement parameters are assessed.

ARTICLE INFO

Article history:
Received 8 May 2014
Received in revised form 8 August 2014
Accepted 22 October 2014
Available online 27 November 2014

Keywords:
Concrete
High-strength concrete (HSC)
Fiber reinforced polymer (FRP)
Columns
Confinement
Shrinkage
Interface gap

ABSTRACT

Fiber reinforced polymer (FRP)-confined concrete has received significant research attention over the last two decades, with recent experimental studies identifying significant benefits of FRP-confined high-strength concrete (HSC). However, studies examining the influence of concrete shrinkage on the behavior of FRP-confined concrete remain limited, with no studies examining this effect for HSC specimens. Concrete shrinkage may pose a concern for concrete-filled FRP tubes (CFFTs), as in these members the curing of concrete takes place inside the FRP tube. This paper presents an experimental investigation on the influence of FRP-to-concrete interface gap, caused by concrete shrinkage, on axial compressive behavior of FRP-confined normal- and high-strength concrete (NSC and HSC). A total of 30 aramid FRP (AFRP)-confined concrete specimens with circular cross-sections were manufactured. Six of the specimens were instrumented to monitor long term shrinkage strain development of the FRP-confined NSC and HSC, with three specimens allocated to each mix. The remaining 24 specimens were tested under axial compression, where nine of these specimens were manufactured with NSC and the remaining 15 with HSC. The influence of concrete shrinkage was examined by applying a gap of up to 0.12 mm thickness at the FRP-to-concrete interface, simulating 1600 microstrain of shrinkage in the radial direction. The results of this experimental study indicate that the influence of interface gap on axial strain enhancement is significant, with an increase observed as the gap increased. Conversely, the influence of interface gap on axial strength enhancement is found to be small with a slight reduction observed with increased gap. The results also indicate that an increase in interface gap causes an increase in strength loss during the transition region of the stress–strain curve as a result of the delayed activation of the FRP shell. Finally, it was observed that an increase in FRP-to-concrete interface gap leads to an increased difference between axial deformation of the concrete core and FRP shell, indicating the presence of interface slip.

1. Introduction

It is now well-understood that the confinement of concrete with fiber reinforced polymer (FRP) composites can lead to significant improvements in both compressive strength and ductility of normal- (e.g., [1–5]) and high-strength (e.g., [6–10]) concretes (NSC and HSC). A large number of experimental studies into the axial compressive behavior have been performed over the last two decades producing over 3000 test results, as discussed and assessed in the recent comprehensive review studies reported in Ozbakkaloglu et al. [11] and Ozbakkaloglu and Lim [12]. These studies revealed that the majority of the existing experimental studies focused on the behavior of FRP-wrapped specimens (e.g.,

* Corresponding author. Tel.: +61 8 8303 6477; fax: +61 8 8303 4359.
E-mail address: togay.ozbakkaloglu@adelaide.edu.au (T. Ozbakkaloglu).

http://dx.doi.org/10.1016/j.conbuildmat.2014.10.038
0950-0618/

[4,8,10,13–18]) with fewer studies reported on concrete-filled FRP tubes (CFFTs). Earlier experimental studies on CFFTs [19–21] along with more recent extensive studies on the axial compressive [7–9,22–29] and seismic behavior of CFFT columns [30–36] have demonstrated the ability of CFFTs to develop very high inelastic deformation capacities, making them an attractive option for construction of new high-performance columns.

The use of higher strength concretes in the construction industry has been on a recent steady incline due to the significantly better structural engineering properties offered by HSC compared with conventional NSC. The use of higher strength concretes in FRP-confined members leads to an efficient combination of two high strength materials to form a high performance member while eliminating the brittle behavior normally associated with HSC. Extensive recent research that has been undertaken by the research group led by the second author on CFFTs manufactured with HSC has demonstrated the ability of high-strength CFFTs (HSCFFTs) to display significant strength and strain enhancements [6–8,26,27,29]. However, the influence of long term concrete shrinkage on the axial compressive behavior of HSCFFTs is yet to be investigated. Concrete shrinkage may pose a concern for CFFT columns, as in these columns the curing of concrete takes place inside the FRP tube. This concrete shrinkage may influence the compressive behavior of the CFFT columns in the long term, and hence it is important to understand this influence for successful design and construction of these members. This is of particular importance for CFFTs manufactured with HSC due to the potential of higher levels of shrinkage associated with higher strength concretes [37,38]. Although a number of studies have been reported on the shrinkage behavior of concrete inside steel tubes (e.g. [39–45]), only two studies have been reported to date on concrete shrinkage in FRP-confined concrete, with both studies examining NSC specimens [46,47]. Naguib and Mirmiran [46] monitored the shrinkage strain development of a single CFFT specimen, where the concrete shrinkage strains were monitored over a 12 month period. However, the influence of shrinkage on the axial compressive behavior of the CFFT was not investigated. Karimi et al. [47] studied the compressive behavior of CFFT specimens with internal steel I-beams manufactured with and without a shrinkage reducing agent. It was reported that the former specimens exhibited approximately 20% higher compressive strengths compared to the latter. To date, no experimental study has investigated the influence of concrete shrinkage on the compressive behavior of CFFTs with the aim of understanding the variations in the behavior with different amounts of concrete shrinkage.

As the first experimental study on FRP-confined concrete to examine the influence of amount of concrete shrinkage, the research program reported in this paper investigated the compressive behavior of NSC and HSC specimens designed with up to five different shrinkage levels in the radial direction. The radial shrinkage was simulated through predetermined gaps ranging from 0 to 0.12 mm supplied at the FRP-to-concrete interface, representing up to 1600 microstrain (με) of concrete shrinkage. The results of the test program are first presented and followed by a detailed discussion on the observed influences of interface gap on specimen behavior.

2. Experimental program

2.1. Test specimens

A total of 30 aramid FRP (AFRP)-confined cylindrical specimens, all with a 152 mm diameter (D) and a 305 mm height (H), were prepared for the two phase experimental program. In the first phase, six specimens were prepared to monitor long term shrinkage development of the concrete in CFFTs. Two different concrete mixes were used, with average compressive strengths of 44.8 and 83.2 MPa which are labeled in this paper as NSC and HSC, respectively. Three of these specimens were manufactured as NSC specimens, with the remaining three specimens manufactured as HSC. These six specimens were prepared as CFFTs to allow shrinkage measurements of FRP-confined concrete to be taken directly after the hardening of concrete. The tubes of the CFFT specimens were manufactured using two layers of AFRP, and the bottom and top surfaces of the specimens remained covered and uncovered respectively, for the entire duration of shrinkage strain measurements.

In the second phase of the experimental program, 24 AFRP-confined cylindrical specimens were prepared and tested under axial compression. The same concrete mixes from Phase 1 were used, with NSC and HSC specimens wrapped with two and four layers of AFRP, respectively. The influence of concrete shrinkage on the compressive behavior of CFFTs was examined by preparing specimens with varying amounts of gap at the FRP-to-concrete interface, simulating the change in interface conditions due to radial shrinkage of concrete. This gap was achieved by wrapping low strength polyethylene sheets around the concrete during the manual wet lay-up procedure of the aramid fiber sheets, to create a boundary gap between the concrete and FRP shell. In this phase of the experimental program, the specimens were manufactured as FRP-wrapped specimens, instead of CFFTs, because this allowed simulation of a constant level of shrinkage in a controlled manner. The concrete specimens were 152 mm in diameter and the polyethylene sheets were 0.03 mm in thickness, resulting in a simulated nominal radial shrinkage of 400 με per layer of polyethylene sheet. The NSC specimens were prepared with nominal shrinkage levels of 0, 400 and 800 με, whereas the HSC specimens had 0, 400, 800, 1200 and 1600 με. These shrinkage levels were selected to represent maximum possible shrinkage strains to be experienced by concrete in a CFFT column and are based on the results obtained from the first phase of the study, as discussed later in the paper. Each concrete cylinder was examined prior to wrapping and all significant concrete surface indentations were leveled with gap filling paste. The details of these the six CFFT specimens and 24 FRP-wrapped test specimens are given in Table 1.

2.2. Materials and specimen preparation

2.2.1. Concrete

Both the NSC and HSC were batched and mixed in the laboratory and consisted of crushed bluestone gravel as the coarse aggregate, with a 10 mm nominal maximum diameter. Superplasticiser was added to the HSC mix to ensure a workable concrete, which resulted in a measured slump of over 220 mm. The in-place concrete strengths (f'_{co}) were established from control cylinders with 100 by 200 mm dimensions cast from the NSC and HSC mixes and tested in parallel to the FRP-confined specimens. The mix designs for the NSC and HSC mixes are reported in Table 2.

2.2.2. FRP and polyethylene

The specimens were manufactured using a wet lay-up technique, which involved wrapping epoxy resin impregnated aramid fiber sheets around either Styrofoam templates or precast concrete cylinders for the CFFT and FRP-wrapped specimens, respectively. The FRP tubes/jackets were prepared using a continuous fiber sheet with fibers oriented in the hoop direction, and they had a single overlap region of 150 mm length. The FRP-wrapped specimens had jackets applied to the precast concrete that had cured for 28 days, and the jackets were cured for at least 7 days before the testing of the specimens. The manufacturer supplied material

Table 1
Details of test specimens.

Testing method	Concrete grade	Average f'_{co}, (MPa)	Fiber thickness, t_f (mm)	Shrinkage gap (με)	Number of specimens
Shrinkage monitoring	NSC	44.8	0.4	Monitored	3
	HSC	83.2	0.4	Monitored	3
Axial compressive testing	NSC	44.8	0.4	0	3
				400	3
				800	3
	HSC	83.2	0.8	0	3
				400	3
				800	3
				1200	3
				1600	3
				Total	30

Table 2
Concrete mix proportions.

Concrete constituent	NSC	HSC
Cement (kg/m^3)	380	506
Silica fume (kg/m^3)	0	44
Sand (kg/m^3)	700	700
Coarse aggregate (kg/m^3)	1050	1050
Water (kg/m^3)	220	172
Superplasticiser (kg/m^3)	0	12
Water to cement ratio	0.58	0.33

properties of the unidirectional aramid fiber sheets and epoxy based adhesive used in the fabrication of the FRP tubes and jackets are shown in Table 3. In addition to manufacturer supplied properties of fiber sheets, the material properties of the FRP composites established through flat coupon tests conducted in accordance with ASTM standard D3039M-08 [48] are supplied in Table 3. The table also displays the material properties of the polyethylene sheets used to create the interface gap. The polyethylene sheets were applied during the FRP wet lay-up process, as illustrated in Fig. 1, and they remained in place throughout the axial compression tests. The polyethylene sheet material properties were established through flat coupon tests conducted in accordance with AS1145.3 [49]. The thickness of the polyethylene sheets were monitored by precision instruments to ensure the required FRP-to-concrete interface gap was maintained. The length of each polyethylene sheet was equal to the circumference of the concrete core so no overlap existed.

2.3. Instrumentation and testing procedure

The six CFFTs used in the first phase of the experimental program were instrumented with strain gauges and placed in a temperature controlled room to monitor the long-term shrinkage strain (ε_{sh}) development of concrete. Each specimen was instrumented with a single 20-mm strain gauge bonded to the center of the top concrete surface. Specimens were placed in a controlled environment, with the temperature maintained at 22 ± 2 °C and relative humidity at 55 ± 10%.

The axial compressive test specimens of Phase 2 were instrumented with four linear variable differential transformers (LVDTs) mounted at the corners between the loading and supporting steel plates of the test machine as shown in Fig. 2. The recorded deformations were used in the calculation of the average axial strains along the height of the specimens. In addition to the four full-height LVDTs (FLVDTs), four mid-section LVDTs (MLVDTs) were mounted on an aluminum cage attached to the mid section of each specimen. This aluminum cage had an LVDT installed on each of its four sides and was designed to mount directly on the FRP shell via surface screws. The LVDT cage had a gauge length of 175 mm and it was placed at equal distance from each specimen end. Fig. 2(c) shows the LVDT cage and the setup used to test the mid-section axial deflection of the FRP shells. These MLVDT strain readings were used to correct the FLVDT measurements at the early stages of loading, where additional displacements due to closure of the gaps in the setup were also recorded by the FLVDTs. Hoop strains around the specimen perimeter were measured by five unidirectional strain gauges having a gauge length of 5 mm that were bonded horizontally on the FRP jacket outside the overlap region at specimen mid-height.

The specimens in Phase 2 were tested under monotonic axial compression using a 5000-kN capacity universal testing machine. The testing of the specimens started immediately after attainment of the 35-day concrete strength and continued for approximately 3 weeks. The loading was applied with load control at 3 kN per second, whereas displacement control was used at approximately 0.005 mm per second beyond the initial softening until specimen failure. To ensure an even loading surface each specimen end was machined using a precision grinding machine before testing.

Table 3
Material properties of fiber, FRP composite, polyethylene sheets and epoxy resin.

Type	Nominal thickness t_f (mm/ply)	Material properties						Epoxy resin properties provided by manufacturer		
		Provided by manufacturer			Obtained from coupon tests					
		Ultimate tensile stress f_f (MPa)	Ultimate tensile strain ε_{fu} (%)	Elastic modulus E_f (GPa)	Ultimate tensile stress f (MPa)	Ultimate tensile strain ε (%)	Elastic modulus E (GPa)	Ultimate tensile stress f_{epoxy} (MPa)	Yield strain ε_{epoxy} (%)	Elastic modulus E_{epoxy} (GPa)
Aramid fiber	0.2	2600	2.20	118.2	2390[a]	1.86	128.5[a]	–	–	–
Polyethylene sheet	0.03	–	–	–	18.6	209	0.15	–	–	–
Epoxy resin	–	–	–	–	–	–	–	>50	2.5	>3

[a] calculated based on nominal thickness of fibers in FRP coupons.

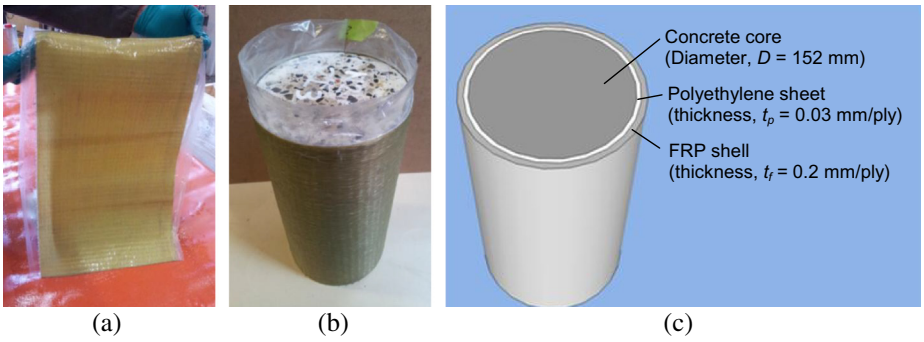

Fig. 1. Implementing gap effect on FRP-wrapped concrete cylinders: (a) polyethylene and FRP sheet before wrapping; (b) wrapped specimen; and (c) technical illustration.

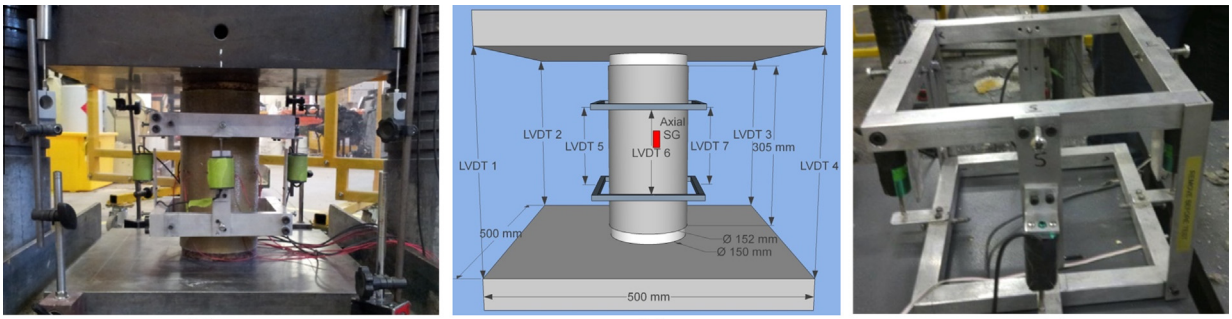

Fig. 2. Instrumentation of specimens: (a) specimen before testing; (b) technical illustration; and (c) mid-section LVDT cage.

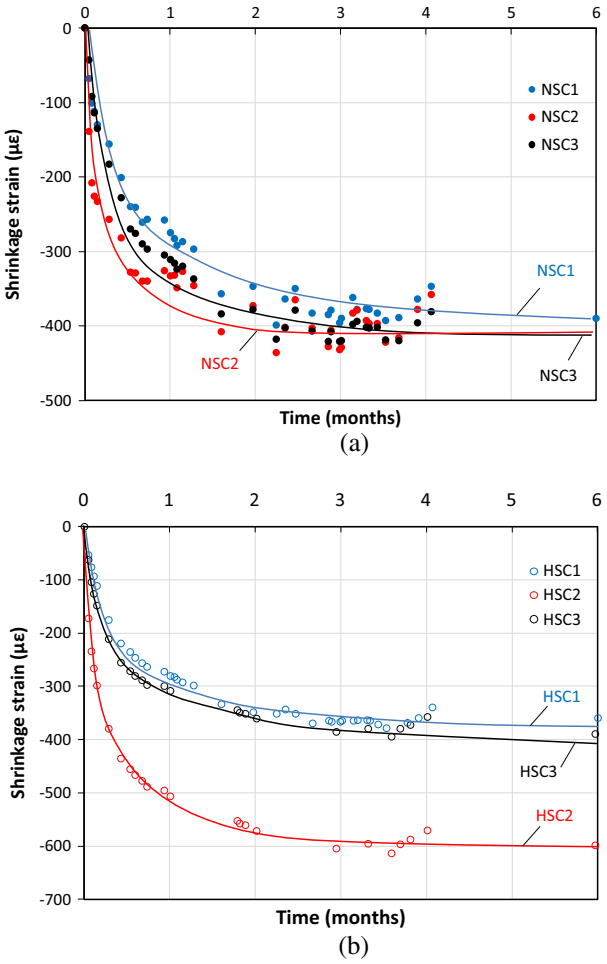

Fig. 3. Shrinkage of concrete in CFFTs: (a) NSC; and (b) HSC.

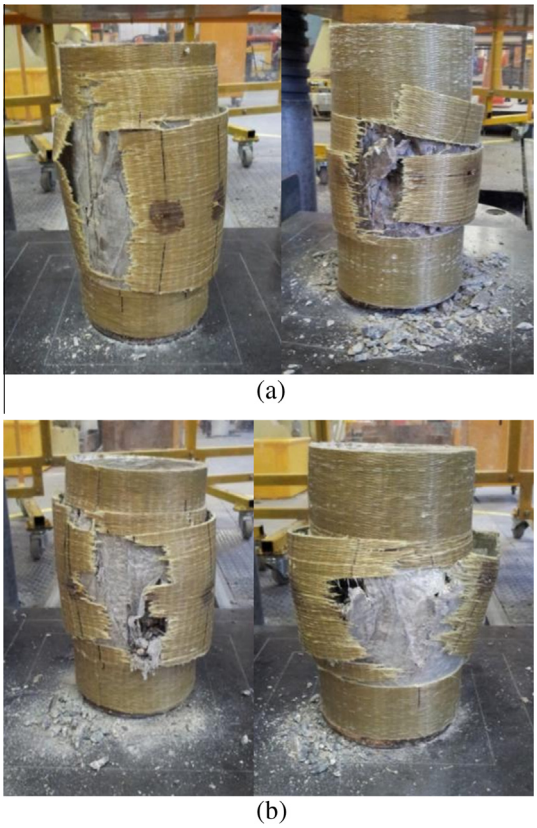

Fig. 4. Typical failures of axial compression test specimens (a) NSC specimens; and (b) HSC specimens.

Table 4
Test results.

Concrete grade	Specimen	f'_{co} (MPa)	$f_{lu,a}/f'_{co}$	f'_{cc} (MPa)	ε_{cu} (%)	$\varepsilon_{h,rup}$ (%)	f'_{cc}/f'_{co}	$\varepsilon_{cu}/\varepsilon_{co}$	k_ε
NSC	N-0.4T-0-1[a]	44.8	–	78.3	2.15	–	1.68	7.83	0.81
	N-0.4T-0-2	44.8	0.25	73.4	1.78	1.79			
	N-0.4T-0-3[a]	44.8	–	74.5	1.77	–			
	N-0.4T-400-1	44.8	0.21	73.5	2.18	1.49	1.67	9.13	0.85
	N-0.4T-400-2	44.8	0.27	72.3	2.17	1.93			
	N-0.4T-400-3	44.8	0.30	78.7	2.29	2.18			
	N-0.4T-800-1	44.8	0.24	70.9	2.42	1.74	1.61	10.39	0.83
	N-0.4T-800-2	44.8	0.25	75.6	2.59	1.81			
	N-0.4T-800-3	44.8	0.26	69.6	2.55	1.90			
HSC	H-0.8T-0-1	83.2	0.22	133.7	1.77	1.49	1.64	6.39	0.68
	H-0.8T-0-2	83.2	0.23	136.8	1.72	1.53			
	H-0.8T-0-3	83.2	0.22	139.1	1.93	1.47			
	H-0.8T-400-1	83.2	0.24	128.7	2.44	1.60	1.59	8.35	0.75
	H-0.8T-400-2	83.2	0.23	129.7	2.37	1.57			
	H-0.8T-400-3	83.2	0.27	138.4	2.28	1.81			
	H-0.8T-800-1	83.2	0.25	137.5	2.86	1.65	1.54	8.95	0.72
	H-0.8T-800-2	83.2	0.22	125.5	2.40	1.49			
	H-0.8T-800-3	83.2	0.24	121.6	2.33	1.59			
	H-0.8T-1200-1	83.2	0.22	116.6	2.29	1.49	1.46	8.50	0.73
	H-0.8T-1200-2	83.2	0.27	137.0	2.61	1.78			
	H-0.8T-1200-3	83.2	0.23	110.3	2.32	1.52			
	H-0.8T-1600-1	83.2	0.24	121.1	2.45	1.63	1.51	9.40	0.72
	H-0.8T-1600-2	83.2	0.21	121.4	2.85	1.40			
	H-0.8T-1600-3	83.2	0.26	135.0	2.68	1.71			

[a] Indicates specimen experienced problems with acquisition of lateral strain data.

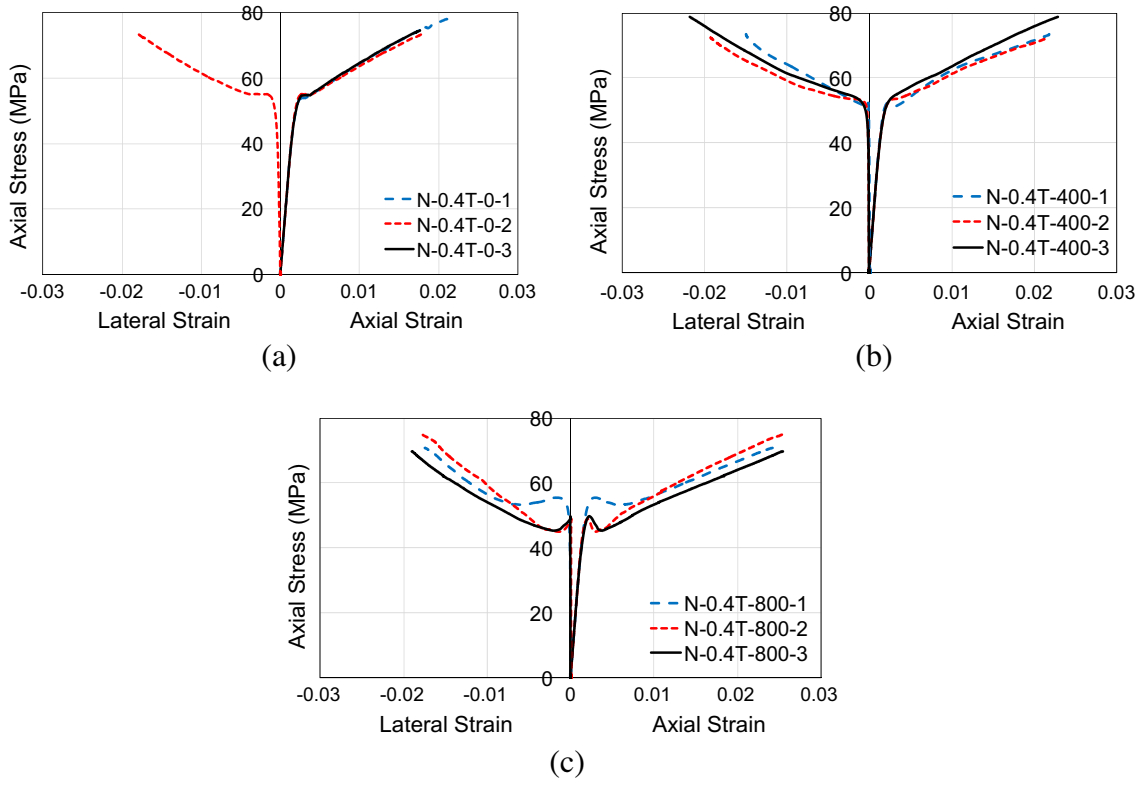

Fig. 5. Axial stress–strain behavior of NSC specimens: (a) no interface gap; (b) 400 με interface gap; and (c) 800 με interface gap.

Precision cut steel discs, 15-mm thick and 150-mm in diameter, were installed at specimen ends to apply the load only to the concrete core.

2.4. Specimen designation

The specimens presented in Table 1 were labeled according to concrete grade, confinement amount and interface shrinkage gap. For the first parameter, letters N and H were used to signify the use of either normal- or high-strength concrete. The confinement amount was then given indicating the total nominal thickness of the fibers in millimeters followed by the letter T. Next the interface shrinkage gap was given indicating the total shrinkage in με. Finally, a number was used to distinguish between nominally identical specimens. For example 'H-0.8T-1200-3' relates to an HSC specimen confined by a total fiber thickness of 0.8 mm with an

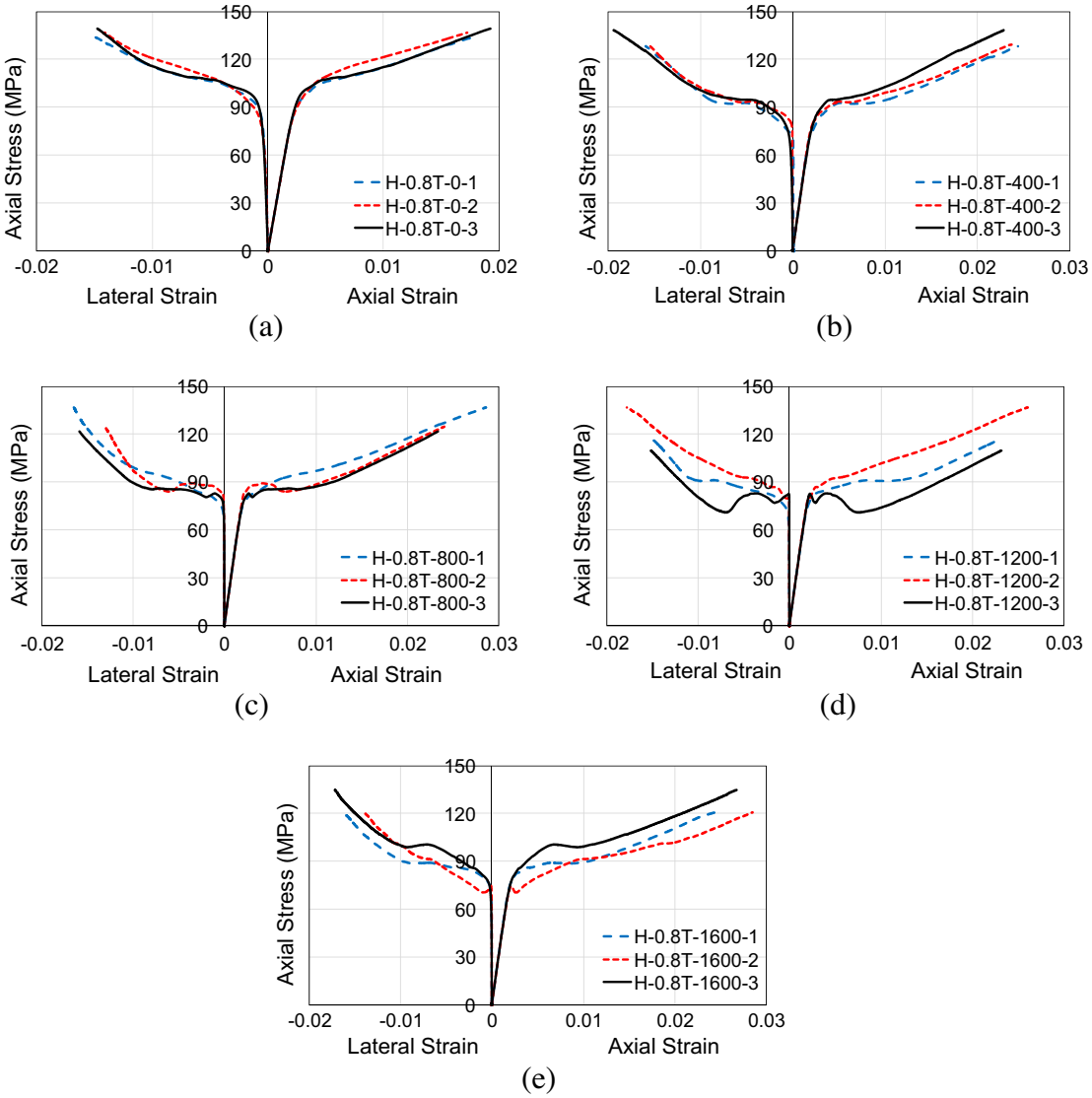

Fig. 6. Axial stress to lateral- and axial-strain behavior of HSC specimens: (a) no interface gap; (b) 400 με interface gap; (c) 800 με interface gap; (d) 1200 με interface gap; and (e) 1600 με interface gap.

interface shrinkage gap of 1200 με and is the third specimen in its group.

3. Test results

3.1. Shrinkage strain measurements

The concrete shrinkage strain (ε_{sh}) measurements of the NSC and HSC specimens from the first phase of the study are presented in Fig. 3. The figure illustrates the concrete shrinkage strain development at the top surface of the CFFTs, which were capped at their bottom surfaces. The shrinkage strains were monitored over a period of 6 months to establish early shrinkage strain behavior. Measurements of shrinkage strains began immediately after strain gauges were mounted to the top surface of the hardened concrete, approximately 24 h after the concrete was cast into the FRP tubes. These recorded values of shrinkage strain were extrapolated to obtain the maximum shrinkage strains expected over the full service life of a CFFT column and the corresponding gaps to be applied to the specimens of Phase 2.

3.2. Axial compression tests

3.2.1. Observed failure modes

The observed failure mode of the 24 NSC and HSC specimens was rupture of the FRP tube accompanied by an instantaneous loss of applied load. The observed FRP rupture of all specimens was characterized by localized segmented rupture occurring at the specimen mid-section. Typical failures of the specimens are shown in Fig. 4, where examples of observed failure modes of NSC and HSC specimens are provided. Typical shear cone formations were evident in all failed specimens where FRP rupture allowed examination of the concrete core.

3.2.2. Stress–strain behavior and ultimate condition

The ultimate condition, which consists of the ultimate axial stress (f'_{cc}) recorded at failure of the specimen, corresponding axial strain (ε_{cu}) and FRP hoop rupture strain ($\varepsilon_{h,rup}$), of each of the 24 test specimens is reported in Table 4. The table also reports group averages of axial strength and strain enhancement ratios (f'_{cc}/f'_{co} and $\varepsilon_{cu}/\varepsilon_{co}$), where ε_{co} was determined using the expression proposed by Popovics [50]. The complete stress–strain relation-

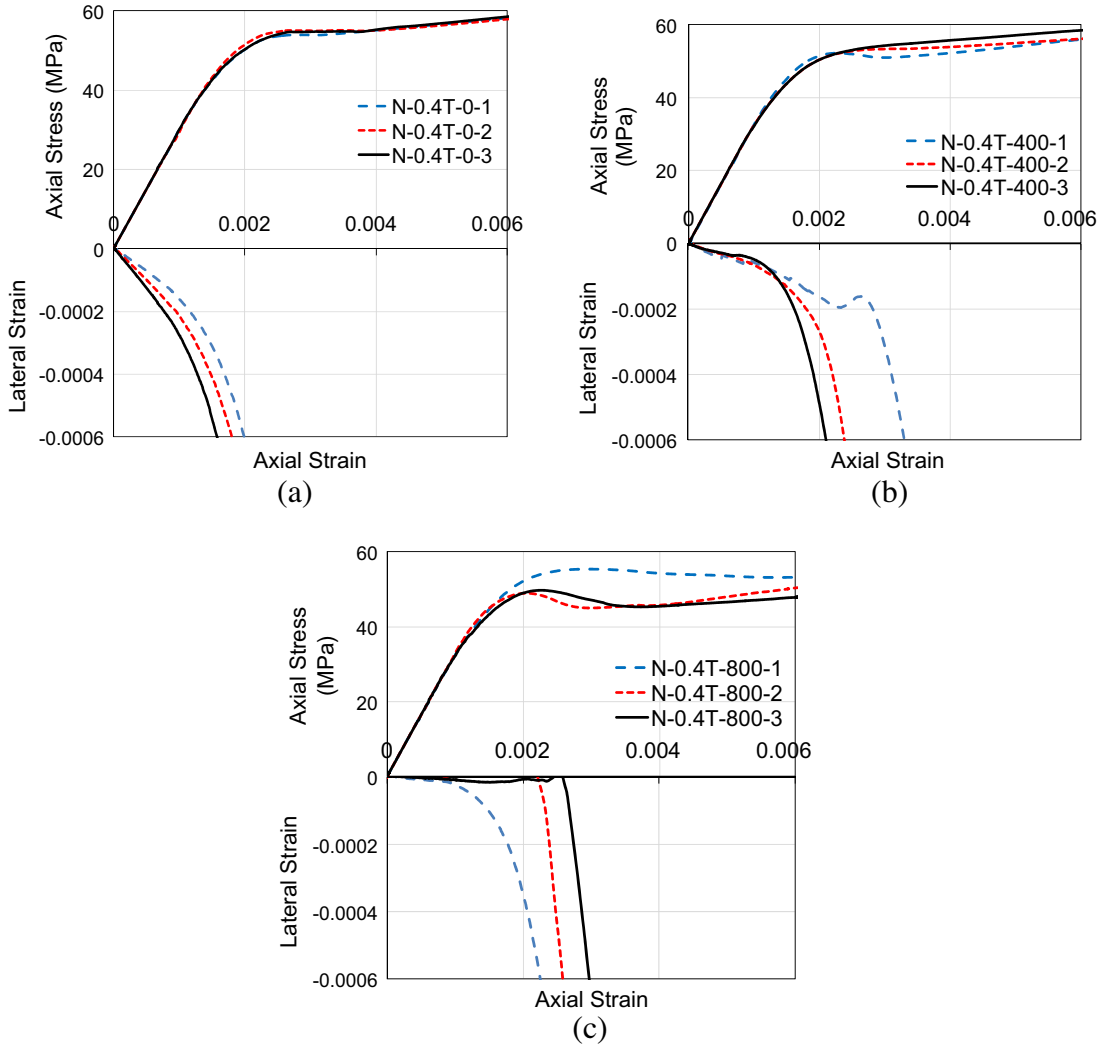

Fig. 7. Lateral-to-axial strain and corresponding axial stress–strain relationships of NSC specimens: (a) no interface gap; (b) 400 με interface gap; and (c) 800 με interface gap.

ships of the NSC and HSC specimens are shown in Figs. 5 and 6, respectively, which illustrate the variation of lateral and axial strains with axial stress. The ultimate axial strains (ε_{cu}) reported in Table 4 and the stress–strain curves given in Figs. 5 and 6 were established from the four FLVDTs with corrections supplied from the four MLVDTs, as mentioned previously. Figs. 7 and 8, respectively, present the lateral-to-axial strain relationships together with the corresponding axial stress–strain relationship for the NSC and HSC specimens. In these figures the initial branch of the stress–strain curve is displayed to illustrate the lateral strain development up to, and including, the transition region where the concrete rapidly expands and activates the FRP-confinement shell.

It is now well-understood that the hoop rupture strains ($\varepsilon_{h,rup}$) recorded in FRP-confined concrete specimens are often smaller than the ultimate tensile strain of the fibers (ε_{fu}) reported by the manufacturer [10,23,51–53]. The average strain reduction factors k_ε, determined from Eq. (1), was established for each group of identical test specimens and are presented in Table 4. To ensure reliability, plots of hoop strain development were examined and unreliable strain gauge readings, caused by instrumentation problems or partial strain gauge debonding due to localized damages, were omitted.

$$k_\varepsilon = \frac{\varepsilon_{h,rup}}{\varepsilon_{fu}} \tag{1}$$

4. Analysis of test results

4.1. Shrinkage behavior

It can be seen from the shrinkage strains (ε_{sh}) of the NSCFFTs shown in Fig. 3(a) that NSC specimens recorded approximately 400 με of radial shrinkage after six months, with over 85% of this occurring during the first two months. A similar shrinkage behavior was evident for the HSC specimens shown in Fig. 3(b), with a maximum of around 600 με of shrinkage recorded at the end of the six-month period. It might be worth noting that these strains recorded on the concrete surface represent the highest shrinkage strains expected to be experienced by the concrete in CFFTs, as the concrete below the top surface is sealed inside the FRP tube resulting in less water loss and lower internal shrinkage strains. Based on the shrinkage strain development trends observed in Fig. 3, FRP-to-concrete interface gaps were selected for the second phase of the experimental program to represent the range of shrinkage expected over the full service life of a NSC- and HSC-FFT column.

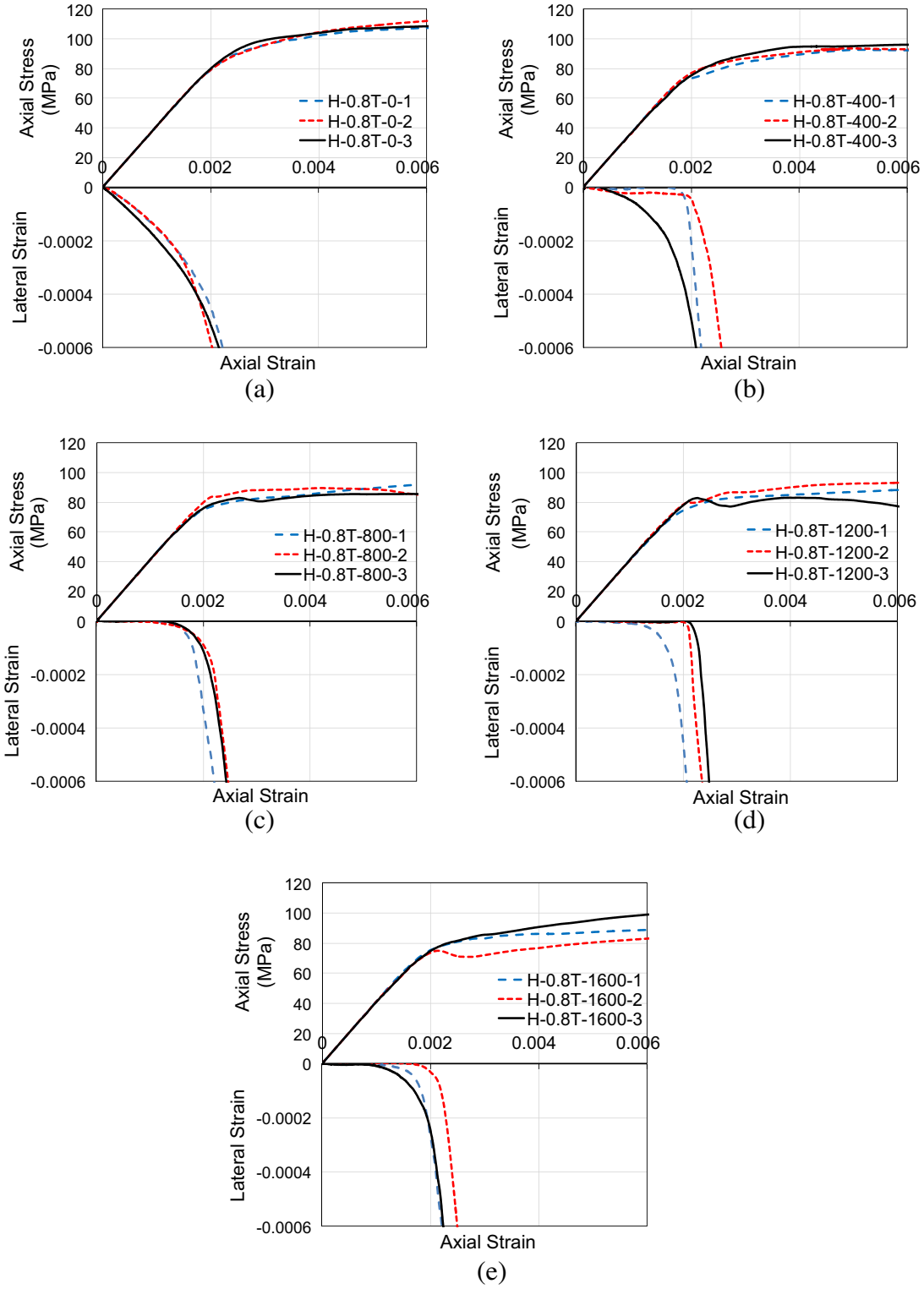

Fig. 8. Lateral-to-axial strain and corresponding axial stress–strain relationships of HSC specimens: (a) no interface gap; (b) 400 με interface gap; (c) 800 με interface gap; (d) 1200 με interface gap; and (e) 1600 με interface gap.

Increments of 400 με were adopted for both concrete grades, with NSC and HSC specimens designed to have maximum 800 and 1600 με of simulated concrete shrinkage in the radial direction. It is worth noting that previous research showed that shrinkage strains of the concrete confined by FRP tubes was around 10–20% of that of exposed concrete [46,47], with comparable values reported for concrete confined by steel tubes [40]. Therefore, the levels of shrinkage considered in this study are believed to be higher than the typical concrete shrinkage strains expected in actual CFFT members, and they represent maximum shrinkage strains expected within localized regions of CFFT members, such as those exposed during stages of construction.

Table 5
Influence of f'_{co} and interface gap on strength and strain enhancement of specimens.

Shrinkage strain (με)	Concrete grade	k_1	k_2
0	NSC	2.24	22.4
	HSC	1.95	16.4
400	NSC	2.20	26.6
	HSC	1.79	22.3
800	NSC	1.99	30.7
	HSC	1.64	24.2
1200	HSC	1.39	22.8
1600	HSC	1.56	25.5

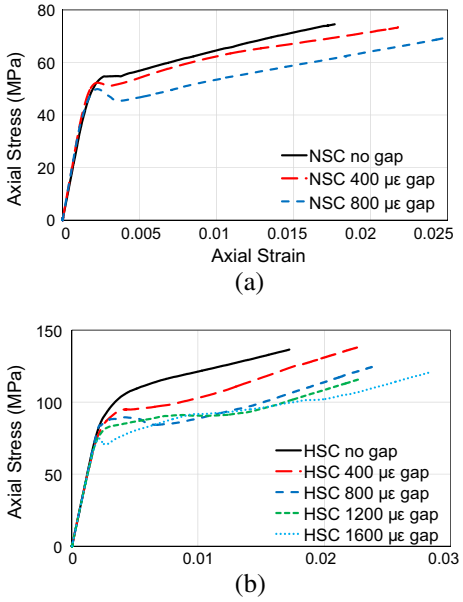

Fig. 9. Influence of interface gap on stress–strain behavior of FRP-confined concrete. (a) NSC; and (b) HSC.

4.2. Axial compressive behavior

4.2.1. Ultimate condition

It can be seen in Table 4 that both NSC and HSC specimens exhibited significant strength and strain enhancements for all levels of examined interface gaps. The table also illustrates that strength and strain enhancement ratios (f'_{cc}/f'_{co} and $\varepsilon_{cu}/\varepsilon_{co}$) are both influenced by presence and size of the interface gap. Table 5 presents a summary of these ultimate conditions where strength and strain enhancement coefficients (k_1 and k_2) are reported. These strength and strain enhancement coefficients were established from Eqs. (2) and (3) respectively, where the actual confinement ratio ($f_{lu,a}/f'_{co}$), defined as the ratio of the actual confining pressure at ultimate ($f_{lu,a}$) to concrete compressive strength (f'_{co}), was calculated from Eq. (4) assuming a uniform confinement pressure distribution.

$$\frac{f'_{cc}}{f'_{co}} = 1.0 + k_1 \frac{f_{lu,a}}{f'_{co}} \tag{2}$$

$$\frac{\varepsilon_{cc}}{\varepsilon_{co}} = 1.0 + k_2 \frac{f_{lu,a}}{f'_{co}} \tag{3}$$

$$\frac{f_{lu,a}}{f'_{co}} = \frac{2t_f E_f \varepsilon_{h,rup}}{f'_{co} D} \tag{4}$$

where t_f is the total nominal thickness of the fibers, E_f is the modulus of elasticity of the fibers, and D is the specimen diameter measured at the concrete core.

The influence of FRP-to-concrete interface gap on the ultimate condition was examined by comparing specimens with the same concrete grade (NSC or HSC) and different interface gap. As evident from Table 5, an increase in FRP-to-concrete interface gap leads to a slight decrease in strength enhancement coefficient (k_1) for both NSC and HSC. On the other hand an increase in interface gap results in a significant increase in strain enhancement coefficient (k_2) for both concrete grades. A comparison of the reported hoop rupture strains ($\varepsilon_{h,rup}$) and corresponding strain reduction factors (k_ε) of the specimens in Table 4 reveals very similar values for a given concrete grade, indicating that the interface gap had only a minor influence on $\varepsilon_{h,rup}$.

The influence of concrete compressive strength (f'_{co}) on specimens with varying amounts of interface gap was investigated by comparing the results reported in Table 5. It can be seen in this table that an increase in concrete compressive strength leads to an overall decrease in both strength enhancement coefficient (k_1) and strain enhancement coefficient (k_2). Table 5 also indicates that similar reductions in k_1 or k_2 were observed for all NSC–HSC specimen pairs having the same interface gaps, indicating that NSC and HSC specimens were influenced by interface gap in a similar manner. A comparison of the strain reduction factors (k_ε) presented in Table 4 reveals that values of k_ε for HSC specimens were significantly lower than those of their NSC counterparts for all levels of interface gaps. These observed influences of concrete strength on ultimate conditions are in agreement with those reported in Ozbakkaloglu and Vincent [7] based on a significantly larger database, and they can be attributed to the change in cracking pattern of concrete with a change in its strength, as previously explained in Ozbakkaloglu and Lim [12].

4.2.2. Axial stress–strain behavior

It can be seen from the axial stress–strain relationships presented in Figs. 5 and 6 that the curves of all specimens exhibited overall ascending second branches. However, it can be observed in these figures that as the interface gap increased so did the tendency for a slight loss in axial stress during the transition region between the first and second branches. Examples of this behavior can be seen for the specimens in the groups N-0.4T-800, H-0.8T-1200 and H-0.8T-1600 shown in Figs. 5(c) and 6(d) and (e), respectively. This behavior can be attributed to the increased interface gap causing a delayed activation of the confinement mechanism, during the rapid expansion of the concrete core. As can be seen in Figs. 5 and 6, this behavior was temporary and was followed by strength recovery and further performance gains. This observation on stress drop due to increased interface gap is in agreement with experimental observations reported in Liu et al. [42] and Xue et al. [41] for concrete-filled steel tubes (CFSTs), which were also supported by the results of the FEA analysis reported in Shiming and Huifeng [44].

Comparison of the stress–strain curves of the companion specimens shown in Fig. 9 illustrates the influence of interface gap on the axial stress–strain behavior of the NSC and HSC specimens. The previously noted influence of the interface gap on ultimate strength and strain (f'_{cc} and ε_{cu}) is evident in Fig. 9, where it can also be seen that the slopes of the second branches remain similar among specimens with the same concrete grade. Fig. 9 further illustrates that as the interface gap increases so does the tendency for a drop in axial strength, starting at the transition point between the first and second branches on the stress–strain curves. As can be seen the figure, this temporary loss in strength was experienced by both NSC and HSC specimens and it was followed by a recovery and subsequent additional gains in strength. This observation sug-

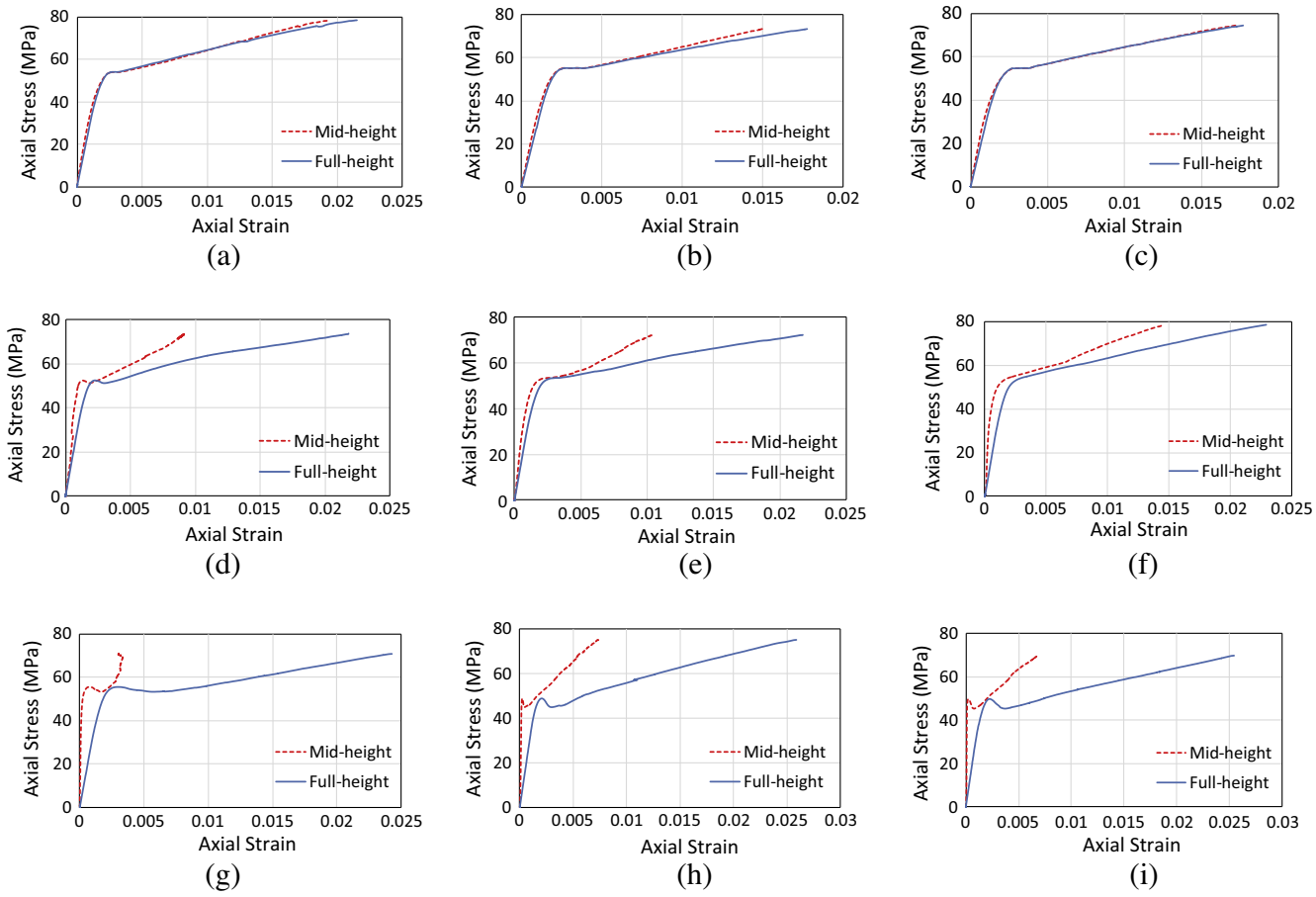

Fig. 10. Influence of instrumentation arrangement on axial stress–strain curves of NSC specimens: (a) N-0.4T-0-1; (b) N-0.4T-0-2; (c) N-0.4T-0-3; (d) N-0.4T-400-1; (e) N-0.4T-400-2; (f) N-0.4T-400-3; (g) N-0.4T-800-1; (h) N-0.4T-800-2; and (i) N-0.4T-800-3.

gests a strong correlation between amount of concrete shrinkage and amount of temporary strength loss during the transition region on the stress strain curve. Further to this, the aforementioned observations on the ultimate conditions suggest that existing stress–strain models, which were developed on the basis of the results from specimens with no gaps, would overestimate the ultimate axial stresses (f'_{cc}) of CFFTs exhibiting radial concrete shrinkage, whereas they would underestimate the ultimate axial strains (ε_{cu}) of these columns.

4.2.3. Lateral strain development on FRP shell

Figs. 7 and 8 present the lateral strain development in the FRP shell and the corresponding stress–strain behavior of the initial branch and transition region for the NSC and HSC specimens, respectively. It can be seen in these figures that specimens with no interface gap started developing lateral strain in the FRP shell as soon as the axial load was applied. On the other hand, specimens with 400 με or higher of interface gaps experienced a significant delay in lateral strain development as the interface gap was closed by the expanding concrete core. It is evident from Figs. 7 and 8 that an increased delay in activation of the lateral confinement effects of the FRP shell led to an increased drop in axial stresses of these specimens along the transition regions of their stress–strain curves. For example, comparison of specimen series H-0.8T-0 and H-0.8T-1600 in Fig. 8(a) and (e) reveals that the H-0.8T-0 series specimens experienced little to no stress drop with their FRP shell being activated during the initial branch. On the other hand, H-0.8T-1600 series specimens experienced a plateau or drop in axial stress during the transition region, as the FRP shell had a significant delay in activation. This observation suggests that a strong correlation exists between delay in FRP activation, as indicated by lateral strain development, and drop in axial stress near the transition region.

4.2.4. Axial strain development on FRP shell

As was previously discussed in Ozbakkaloglu and Lim [12] the recorded ultimate axial strains (ε_{cu}) are highly sensitive to the type of instrumentation used in their measurement. Based on a large database of experimental results, it was shown that LVDTs mounted along the entire height of the specimens (FLVDTs) in general gave higher axial strains than those measured by LVDTs mounted at mid-section of the specimens (MLVDTs). In the present study, the discrepancies between the axial strains obtained from these two instrumentation arrangements were experimentally investigated. As mentioned previously, FLVDT and MLVDT measurements were obtained from LVDTs attached to the loading platens and FRP shell, respectively, and the axial load was applied only to the concrete core. Figs. 10 and 11 display the axial stress–strain curves obtained using the two different measurement methods for the NSC and HSC specimens, respectively, and Table 6 presents a summary of the ultimate axial strains (ε_{cu}) determined from each instrumentation arrangement. It is evident from these figures and table that significant differences may exist between the axial strains measured by these two methods.

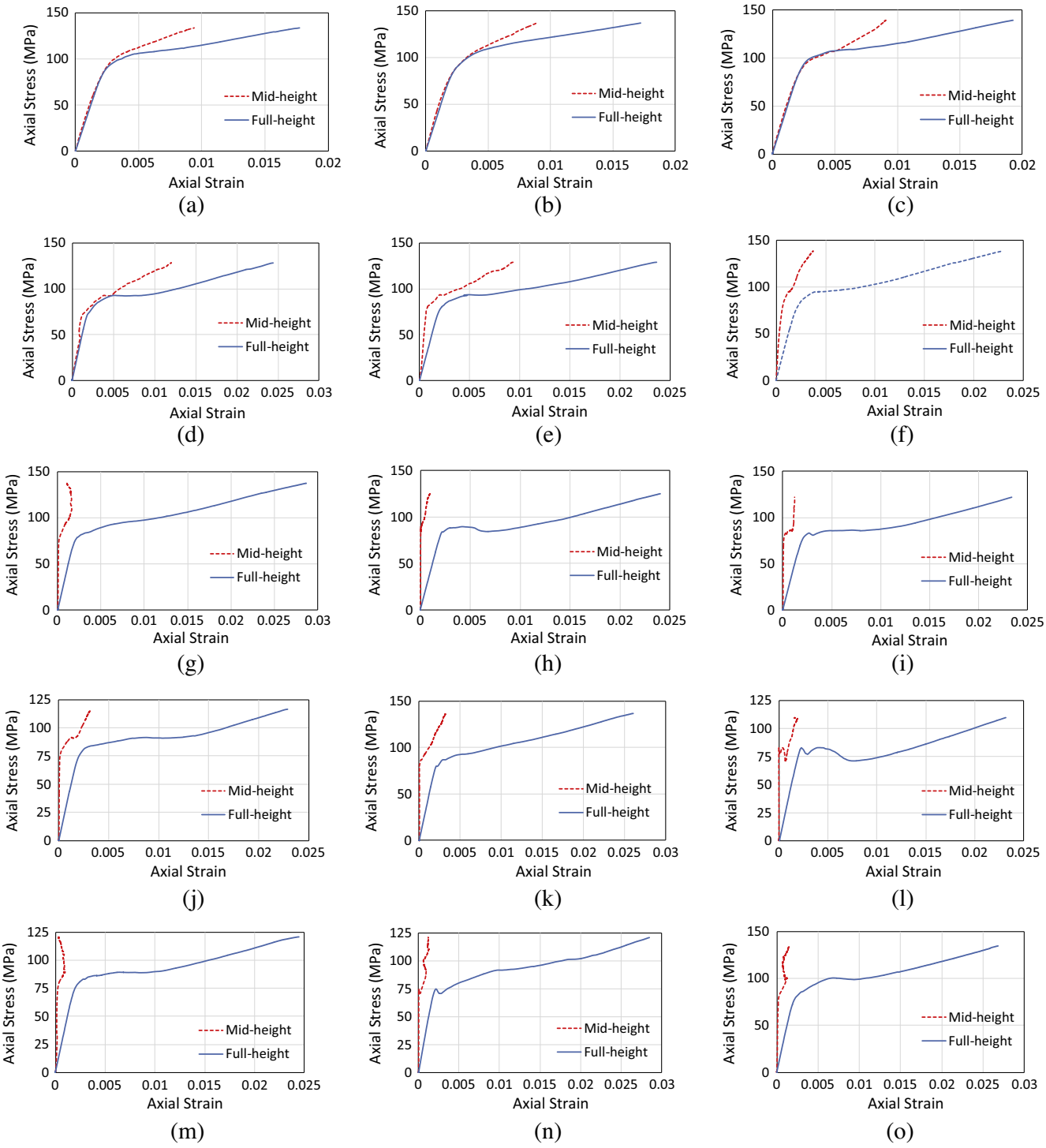

Fig. 11. Influence of instrumentation arrangement on axial stress–strain curves of HSC specimens: (a) H-0.8T-0-1; (b) H-0.8T-0-2; (c) H-0.8T-0-3; (d) H-0.8T-400-1; (e) H-0.8T-400-2; (f) H-0.8T-400-3; (g) H-0.8T-800-1; (h) H-0.8T-800-2; (i) H-0.8T-800-3; (j) H-0.8T-1200-1; (k) H-0.8T-1200-2; (l) H-0.8T-1200-3; (m) H-0.8T-1600-1; (n) H-0.8T-1600-2; and (o) H-0.8T-1600-3.

An examination of the results for specimens with no interface gap, presented in Table 6 and Figs. 10(a)–(c) and 11(a)–(c), reveals that the difference between axial strains obtained from MLVDT and FLVDT is more significant in HSC specimens compared to the companion NSC specimens. In these comparisons it can be seen that the stress–strain curves obtained from MLVDTs and FLVDTs for NSC are quite similar along the entire curve, whereas significant differences exist in the curves of HSC specimens obtained from the two measurement methods beyond the initial peak. This observed difference between NSC and HSC specimens can be attributed to the increased concrete brittleness with increasing concrete strength, which alters the concrete crack patterns from heterogenic microcracks to localized macrocracks as discussed in Ozbakkaloglu and Lim [12]. These macrocracks lead to localized

Table 6
Comparison of axial strains measured by different methods.

Concrete grade	Specimen	ε_{cu} (%)		Average ε_{cu} (%)		MLVDT/FLVDT
		FLVDTs	MLVDTs	FLVDTs	MLVDTs	
NSC	N-0.4T-0-1	2.15	1.94	1.90	1.72	0.91
	N-0.4T-0-2	1.78	1.50			
	N-0.4T-0-3	1.77	1.72			
	N-0.4T-400-1	2.18	0.92	2.21	1.14	0.49
	N-0.4T-400-2	2.17	1.04			
	N-0.4T-400-3	2.29	1.46			
	N-0.4T-800-1	2.42	0.30	2.52	0.60	0.24
	N-0.4T-800-2	2.59	0.79			
	N-0.4T-800-3	2.55	0.69			
HSC	H-0.8T-0-1	1.77	0.94	1.81	0.91	0.50
	H-0.8T-0-2	1.72	0.89			
	H-0.8T-0-3	1.93	0.91			
	H-0.8T-400-1	2.44	1.20	2.36	0.84	0.35
	H-0.8T-400-2	2.37	0.93			
	H-0.8T-400-3	2.28	0.37			
	H-0.8T-800-1	2.86	0.11	2.53	0.11	0.04
	H-0.8T-800-2	2.40	0.10			
	H-0.8T-800-3	2.33	0.12			
	H-0.8T-1200-1	2.29	0.32	2.41	0.27	0.11
	H-0.8T-1200-2	2.61	0.32			
	H-0.8T-1200-3	2.32	0.16			
	H-0.8T-1600-1	2.45	0.03	2.66	0.10	0.04
	H-0.8T-1600-2	2.85	0.12			
	H-0.8T-1600-3	2.68	0.16			

regions of post-peak plastic deformations, which may be formed completely or partially outside the mid-height region. As a result, in HSC specimens the mid-section LVDTs are unable to fully capture these post peak deformations, resulting in lower ultimate axial strain measurements compared to the full-height LVDTs.

The influence of concrete compressive strength (f'_{co}) and interface gap on the difference between axial strains obtained from MLVDT and FLVDT measurement method can be examined in Table 6 and Figs. 10 and 11. Similar to the observation on specimens with no gap, it can be seen in Table 6 that specimens with comparable interface gaps experience a significant decrease in MLVDT/FLVDT with an increase in concrete compressive strength (f'_{co}). The results in Table 6 also indicate a strong correlation between FRP-to-concrete interface gap and MLVDT/FLVDT ratio. It can be seen in the table that, for a given concrete grade, an increase in interface gap leads to a significant decrease in MLVDT/FLVDT ratio. The observed influence of interface gap on axial strain measurements can be attributed to the partial or complete loss of bond at the interface between the concrete core and FRP shell. It can be seen in Fig. 11 that a complete loss of bond is evident for HSC specimens with 800 με or larger interface gaps. It is worth noting that the bond behavior of the FRP-to-concrete interface might have been influenced by the change in the friction coefficient on the interface surfaces due to the provision of the polyethylene sheets, and hence the effect may not be limited exclusively to the size of FRP-to-concrete interface gap. It is worth further noting that the aforementioned change in FRP-to-concrete bond condition might have had some influence on the axial stress–strain behaviors of the specimens, as the interface bond condition affects the axial loading condition of the FRP tube. Additional experimental studies are required to further investigate the influences of FRP-to-concrete interface gap and interface friction coefficient on the compressive behavior of FRP-confined concrete.

5. Conclusions

This paper has reported the results of an experimental investigation into the influence of FRP-to-concrete interface gap on the compressive behavior of FRP-confined concrete. Based on the results and discussion presented in this paper, the following conclusions can be drawn:

1. An increase in FRP-to-concrete interface gap results in a slight decrease in strength enhancement ratio (f'_{cu}/f'_{co}), whereas it leads to a significant increase in strain enhancement ratio ($\varepsilon_{cu}/\varepsilon_{co}$). It is observed that the interface gap affects the strength and strain enhancement ratios of NSC and HSC in a similar manner, suggesting that the influence is independent of concrete compressive strength (f'_{co}).
2. For a given concrete strength (f'_{co}), FRP-to-concrete interface gap has no major influence on hoop rupture strain ($\varepsilon_{h,rup}$). On the other hand, $\varepsilon_{h,rup}$ is influenced significantly by concrete compressive strength (f'_{co}), with an increase in concrete strength leading to a decrease in $\varepsilon_{h,rup}$ independent of the interface gap.
3. An increase in interface gap increases the tendency for a drop in axial strength at the transition point between the first and second branches of the stress–strain curve of FRP-confined concrete. This strength loss is caused by the delay in activation of the confinement mechanism in the presence of the interface gap.
4. In specimens with no interface gap, the axial strains obtained by LVDTs placed along the full height of the specimen are higher than those measured by LVDTs mounted at specimen mid-section. This difference is dependent on the concrete strength (f'_{co}), and it is small for NSC specimens but significant for HSC specimens.
5. An increase in the FRP-to-concrete interface gap results in a significant decrease in the ratio of the ultimate axial strains obtained from mid-section and full-height LVDTs (MLVDT/FLVDT) due to a partial or complete loss of bond at the interface between the concrete core and FRP shell.

References

[1] Fam AZ, Rizkalla SH. Confinement model for axially loaded concrete confined by circular fiber-reinforced polymer tubes. ACI Struct J 2001;98(4):451–61.

[2] Karabinis AI, Rousakis TC. Concrete confined by FRP material: a plasticity approach. Eng Struct 2002;24(7):923–32.
[3] Jiang T, Teng JG. Analysis-oriented stress-strain models for FRP-confined concrete. Eng Struct 2007;29(11):2968–86.
[4] Ilki A, Onder P, Karamuk E, Demir C, Kumbasar N. FRP retrofit of low and medium strength circular and rectangular reinforced concrete columns. ASCE J Mater Civ Eng 2008;20(2):169–88.
[5] Wu YF, Wei YY. Effect of cross-sectional aspect ratio on the strength of CFRP-confined rectangular concrete columns. Eng Struct 2010;32:32–45.
[6] Lim JC, Ozbakkaloglu T. Confinement model for FRP-confined high-strength concrete. ASCE JCompos Constr 2013. 10.1061/(ASCE)CC.1943-5614.0000376 (Apr. 1, 2013).
[7] Ozbakkaloglu T, Vincent T. Axial compressive behavior of circular high-strength concrete-filled FRP tubes. ASCE J Compos Constr 2013. http://dx.doi.org/10.1061/(ASCE)CC.1943-5614.0000410.
[8] Vincent T, Ozbakkaloglu T. Influence of concrete strength and confinement method on axial compressive behavior of FRP-confined high- and ultra high-strength concrete. Compos Part B 2013;50:413–28.
[9] Vincent T, Ozbakkaloglu T. Influence of fiber orientation and specimen end condition on axial compressive behavior of FRP-confined concrete. Constr Build Mater 2013;47:814–26.
[10] Ozbakkaloglu T, Akin E. Behavior of FRP-confined normal- and high-strength concrete under cyclic axial compression. ASCE J Compos Constr 2012;16(4):451–63.
[11] Ozbakkaloglu T, Lim JC, Vincent T. FRP-confined concrete in circular sections: review and assessment of the stress–strain models. Eng Struct 2013;49:1068–88.
[12] Ozbakkaloglu T, Lim JC. Axial compressive behavior of FRP-confined concrete: experimental test database and a new design-oriented model. Compos Part B 2013;55:607–34.
[13] Rousakis T, Karabinis A. Substandard reinforced concrete members subjected to compression: FRP confining effects. Mater Struct 2008;41(9):1595–611.
[14] Berthet JF, Ferrier E, Hamelin P. Compressive behavior of concrete externally confined by composite jackets. Part A: experimental study. Constr Build Mater 2005;19(3):223–32.
[15] Wang LM, Wu YF. Effect of corner radius on the performance of CFRP-confined square concrete columns: test. Eng Struct 2008;30(2):493–505.
[16] Eid R, Roy N, Paultre M. Normal- and high-strength concrete circular elements wrapped with FRP composites. ASCE J Compos Constr 2009;13(2):113–24.
[17] Cui C, Sheikh A. Experimental study of normal- and high-strength concrete confined with fiber-reinforced polymers. ASCE J Compos Constr 2010;14(5):553–61.
[18] Xiao Q, Teng JG, Yu T. Behavior and modeling of confined high-strength concrete. ASCE J Compos Constr 2010;14(3):249–59.
[19] Mirmiran A, Shahawy M. Behavior of concrete columns confined by fiber composites. ASCE J Struct Eng 1997;123(5):583–90.
[20] Fam A, Rizkalla S. Behavior of axially loaded concrete-filled circular fiber-reinforced polymer tubes. ACI Struct J 2001;98(3).
[21] Fam A, Flisak B, Rizkalla S. Experimental and analytical modeling of concrete-filled fiber-reinforced polymer tubes subjected to combined bending and axial loads. ACI Struct J 2003;100(4):499–509.
[22] Ozbakkaloglu T, Oehlers DJ. Manufacture and testing of a novel FRP tube confinement system. Eng Struct 2008;30:2448–59.
[23] Ozbakkaloglu T, Oehlers DJ. Concrete-filled square and rectangular FRP tubes under axial compression. ASCE J Compos Constr 2008;12(4):469–77.
[24] Mohamed H, Masmoudi R. Axial load capacity of concrete-filled FRP tube columns: experimental versus predictions. ASCE J Compos Constr 2010;14(2):231–43.
[25] Park JH, Jo BW, Soon SJ, Park SK. Experimental investigation on the structural behavior of concrete filled FRP tubes with/without steel re-bar. KSCE J Civ Eng 2011;15(2):337–45.
[26] Ozbakkaloglu T. Axial compressive behavior of square and rectangular high-strength concrete-filled FRP tubes. ASCE J Compos Constr 2013;17(1):151–61.
[27] Ozbakkaloglu T. Compressive behavior of concrete-filled FRP tube columns: assessment of critical column parameters. Eng Struct 2013;51:151–61.
[28] Ozbakkaloglu T. Concrete-filled FRP tubes: manufacture and testing of new forms designed for improved performance. ASCE J Compos Constr 2013;17(2):280–91.
[29] Ozbakkaloglu T. Behavior of square and rectangular ultra high-strength concrete-filled FRP tubes under axial compression. Compos Part B 2013;54:97–111.
[30] Seible F, Burgueno R, Abdallah MG, Nuismer R. Development of advanced composite carbon shell systems for concrete columns in seismic zones. In: 11th World conference on earthquake engineering. Elsevier Science; 1996. Paper No. 1375.
[31] Yamakawa T, Zhong P, Ohama A. Seismic performance of aramid fiber square tubed concrete columns with metallic and/or non-metallic reinforcement. Reinf Plas Compos 2003;22(13):1221–37.
[32] Zhu Z, Ahmad I, Mirmiran A. Seismic performance of concrete-filled FRP tube columns for bridge substructures. ASCE J Bridge Eng 2006;11(3):359–70.
[33] Ozbakkaloglu T, Saatcioglu M. Seismic behavior of high-strength concrete columns confined by fiber reinforced polymer tubes. ASCE J Compos Constr 2006;10(6):538–49.
[34] Ozbakkaloglu T, Saatcioglu M. Seismic performance of square high-strength concrete columns in stay-in-place formwork. ASCE J Struct Eng 2007;133(1):44–56.
[35] Saatcioglu M, Ozbakkaloglu T, Elnabelsy G. Seismic behavior and design of reinforced concrete columns confined with FRP stay-in-place formwork, vol. 257. ACI special publication; 2008. SP257-09. 149–170.
[36] Idris Y, Ozbakkaloglu T. Seismic behavior of high-strength concrete-filled FRP tube columns. ASCE J Compos Constr 2013;17(6). http://dx.doi.org/10.1061/(ASCE)CC.1943-5614.000038.
[37] Bissonnette B, Pierre P, Pigeon M. Influence of key parameters on drying shrinkage of cementitious materials. Cem Concr Res 1999;29(10):1655–62.
[38] Kwan A, Fung W, Wong H. Shrinkage of high-strength concrete and high-flowability concrete. HKIE Trans 2010;17(3):25–33.
[39] Roeder C, Cameron B, Brown C. Composite action in concrete filled tubes. ASCE J Struct Eng 1999;125(5):477–84.
[40] Ichinose LH, Watanabe E, Nakai H. An experimental study on creep of concrete filled steel pipes. J Construct Steel Res 2001;57(4):453–66.
[41] Xue J, Chen B, Briseghella B. Experimental research on debonding in concrete-filled steel tubes columns subjected to eccentric loading. IABSE Symposium Report 2010; 97(36): 40–7.
[42] Liu XP, Sun Z, Huang HY, Tang S, Tang CH. Research on mechanical properties of separation concrete-filled steel tubes subjected to eccentric compression on non-separation side. Appl Mechan Mater 2012;117:887–92.
[43] Ma YS, Wang YF. Creep of high strength concrete filled steel tube columns. Thin-Walled Struct 2012;53:91–8.
[44] Shiming C, Huifeng Z. Numerical analysis of the axially loaded concrete filled steel tube columns with debonding separation at the steel-concrete interface. Steel Compos Struct 2012;13(3):277–93.
[45] Ranzi G, Leoni G, Zandonini R. State of the art on the time-dependent behaviour of composite steel-concrete structures. J Construct Steel Res 2013;80:252–63.
[46] Naguib W, Mirmiran A. Time-dependent behavior of fiber-reinforced polymer-confined concrete columns under axial loads. ACI Struct J 2002;99(2):142–8.
[47] Karimi K, Tait M, El-Dakhakhni W. Testing and modeling of a novel FRP-encased steel-concrete composite column. Compos Struct 2011;93(5):1463–73.
[48] ASTM. Standard test method for tensile properties of polymer matrix composites materials. D3039-M-08 2008. West Conshohocken, PA.
[49] Standards_Australia. Determination of tensile properties of plastics materials. Part 3: Test conditions for films and sheets. AS 1145.3 – 2001 2001. Sydney, NSW, Australia.
[50] Popovics S. A numerical approach to the complete stress–strain curves for concrete. Cem Concr Res 1973;3(5):583–99.
[51] Pessiki S, Harries KA, Kestner J, Sause R, Ricles JM. The axial behavior of concrete confined with fiber reinforced composite jackets. ASCE J Compos Constr 2001;5(4):237–45.
[52] Ilki A, Kumbasar N. Compressive behavior of carbon fiber composite jacketed concrete with circular and non-circular cross-sections. Earthquake Eng 2003;7(3):381–406.
[53] Lam L, Teng JG. Design-oriented stress-strain model for FRP-confined concrete. Constr Build Mater 2003;17(6&7):471–89.